Electromagnetic Scattering From Foliage Camouflaged Complex Targets

Mojtaba Dehmollaian, *Student Member, IEEE*, and Kamal Sarabandi, *Fellow, IEEE*

***Abstract*—In this paper, a hybrid target–foliage model based on existing electromagnetic techniques is developed to investigate the scattering behavior of hard targets embedded inside a forest canopy at high frequencies. The proposed model is composed of two basic scattering models, one for foliage and the other for the hard targets. The connection between these two models, which accounts for the interaction between the foliage scatterers and the target and vice versa, is accomplished through the application of the reciprocity theorem. Wave penetration through the forest canopy and near-field and far-field scattering from the canopy's constituents is calculated using a coherent discrete scattering model that makes use of realistic tree structures. Calculation of scattering from a hard target illuminated by the reduced incident field and the scattered field of nearby vegetation is carried out using an iterative physical optics (PO) method formulated for fast computation of foliage–target interaction. To reduce the number of iterations, geometrical optics (GO) approximation is initially used for determining the shadowed areas over the hard target when illuminated by individual foliage scatterers. Furthermore, using a scaled measurement system at millimeter-wave frequency, the accuracy of the iterative PO model is demonstrated, employing a complex target that occupies a volume as big as $86\lambda \times 33\lambda \times 20\lambda$.**

***Index Terms*—Electromagnetic (EM) scattering, hybrid solution methods.**

I. Introduction

DETECTION and identification of hard targets camouflaged inside vegetation canopies are among the most challenging problems in remote sensing [1], [2]. Recent advanced capabilities of synthetic aperture radar (SAR) and interferometric SAR sensors such as multifrequency, multibaseline, and multipolarization features have made a wide range of both civilian and military applications possible. Civilian applications include search and detection of archaeological sites, crashed airplanes in forested environments, and foliage attenuation measurements using trihedrals placed under forest canopies. Military and law enforcement applications include detection and identification of foliage-camouflaged vehicles and facilities. To develop effective detection and identification methods for such purposes, the phenomenology of electromagnetic (EM) wave interaction with foliage and hard targets embedded in forest canopies must be thoroughly understood. Basically, a complete sensitivity study of backscattered fields to different parameters such as different realizations of the forest, different incidence angles, polarizations, and frequencies of the incident field will allow for investigation of applicability of novel detection and identification algorithms, as reported in [3]–[5].

EM scattering from targets inside foliage may be studied using three basic approaches, namely: 1) analytical; 2) exact numerical; and 3) experimental/empirical. At very low frequencies, scattering from the forest itself may be rather small, and scattering behavior from the hard target is not much different from that of the target without the forest. In this case, the foliage can simply be modeled as layered homogeneous dielectric media with different effective dielectric constants. EM scattering in stratified media can be analytically solved, and consequently, closed-form expressions for low-frequency scattering from foliage can simply be obtained.

At microwave frequencies, on the other hand, scattering and attenuation from foliage are rather significant, and their effects on total backscatter and foliage-covered target backscatter must be carefully accounted for. For the problem at hand, modeling the forest by randomly distributed particles and solving the problem of scattering from obscured targets inside random media is not sufficiently accurate. It has been observed that backscattering from and attenuation through the forest is significantly affected by the tree structures [6], [7].

Next, exact numerical simulations such as the finite-difference time-domain (FDTD) technique have been suggested for evaluation of scattering from objects inside random media [8] and scattering from forest [9]. The application of brute-force numerical methods is, however, limited to very high frequencies (VHFs) and lower [9]. At microwave frequencies, overall dimensions of a tree are much larger than a wavelength, and therefore, computation of the scattered field from a number of trees and their interaction with the target becomes computationally intractable.

Finally, scattering from targets inside forest can be studied experimentally using radar systems. Experimental and empirical approaches for phenomenological studies are oftentimes rather limiting due to the lack of comprehensive data sets and the accompanying ground truth. Such methods are, however, very useful for proof of concept and demonstrations [10]–[12].

In this paper, we propose an accurate EM model for scattering from foliage-camouflaged targets at microwave frequencies that accounts for first-order near-field foliage and hard target interactions. This model is constructed from a number of analytic EM tools assembled in a unique fashion for fast and accurate computation of scattered fields using well-known EM theorems. To simplify the problem, the scattering domain is

Manuscript received September 7, 2005; revised March 8, 2006. This work was supported by the Army Research Office under Contract DAAD19-02-1-0262.

The authors are with the Radiation Laboratory, Department of Electrical Engineering and Computer Science, University of Michigan, Ann Arbor, MI 48109 USA (e-mail: saraband@eecs.umich.edu).

Digital Object Identifier 10.1109/TGRS.2006.879109

broken into two parts. The first part of the problem is related to the computation of field propagation through and scattering from foliage. The second part of the problem pertains to the characterization of scattering from the target illuminated by the attenuated incident field and the scattered field from all nearby foliage particles. The forest scattering model is based on the coherent scattering model developed previously [7], [13], and the target model is based on high-frequency techniques. The connection between these two scattering domains is accomplished using the reciprocity theorem [14], [15]. To avoid brute-force time-consuming foliage–target scattering interaction by myriads of vegetation particles around the target, an efficient iterative physical optics (PO) approach is implemented [16]–[19]. The main contribution of this paper is in the construction of a comprehensive foliage–target model that is computationally tractable. This model accounts for scattering from foliage, hard target, and near-field interaction of foliage and the hard target.

This paper is organized as follows. An EM scattering model used for the estimation of scattering from and propagation through foliage is addressed in Section II. In Section III, a hybrid geometrical optics (GO) and iterative PO formulation is presented, which provides the induced surface current on a hard target excited by the incident wave and scattered fields from all nearby foliage scatterers. In Section IV, a general formulation based on the reaction theorem is used, which allows for simple calculation of the backscattered field, including first-order target–foliage interaction. Finally, simulation results of camouflaged hard targets are presented in Section V.

II. EM Scattering From Foliage

EM wave scattering from foliage has been investigated intensely through different models [22], [23] and the Michigan Microwave Canopy Scattering Model (MIMICS) [24]. For the problem at hand, a coherent model capable of maintaining the phase is needed. An accurate model based on coherent scattering theory has been proposed recently [7], [13]. In this model, the vegetation canopy is composed of individual dielectric cylinders and thin dielectric disks, which represent tree trunks, branches, and leaves, respectively, arranged in a semideterministic fashion. The simplification is justifiable for tenuous random media composed of lossy scatterers. The single-scattering forest model also includes the interaction of the scatterers with the ground plane, which is modeled by a half-space dielectric layer. This interaction is accounted for through the application of image theory, maintaining only the saddle point contribution. The formulations for calculating the scattering and attenuation caused by vegetation particles are derived analytically using high- and low-frequency techniques [25], [26]. For precise prediction of field behavior inside the canopy, the structure of the trees must be preserved in the forest model. This is done using a fractal-based model (known as Lindenmayer systems) that can generate very complex tree structures with a finite number of structural and botanical parameters.

Field computation must be carried out coherently to preserve the phase of the scattered fields. Such a model is implemented in [7], where scattering from each tree component when illuminated by the mean field is calculated and the total scattering is expressed as the coherent summation of all the scattering contributions. The mean field is computed using Foldy's approximation, which accounts for the phase change as well as extinction due to the scattering and absorption of the tree particles. The model presented in [7] is valid for scenarios where the observation point is outside in the far-field region of the trees. This model is used to compute the backscattered field from the foliage alone. Recently, a more advanced model was developed [13], in which the observation point can be placed inside the forest, possibly in the near field of some scatterers. Scattering formulations for individual scatterers were modified to achieve a uniform scattering solution for scatterers valid from near-field to far-field regions.

The advantages of this model are given as follows: 1) absolute phase response of the field is preserved; 2) the coherent scattering mechanisms are accounted for; 3) tree architecture, which is very important for accurate estimation of field on the target, are taken into account; and 4) near-field scattering from tree constituents have been captured using uniform formulations valid from near-field to far-field regions. The coherent summation of all scattering contributions, including the reflected waves from the ground plane, is computed to find the total field at a given point within the forest canopy. The total field inside the forest, which is composed of attenuated incident field, its reflection from the ground, and the near-field and far-field scattering from the forest components, is used as the excitation source for the hard target.

In an experiment reported in [27], an estimate for the mean value of the one-way foliage attenuation based on 26 sets of measurement is provided, which can be used for foliage model validation. Here, we compare the simulated and the measured cumulative distribution functions (cdfs) for vertically and horizontally polarized waves. The parameters of the pine tree stand described in [27] are used to generate its fractal model. The tree stand parameters are given as follows: tree height is 14 m, crown thickness is 3.9 m, the average diameter at breast height (dbh) is 19.8 cm, the stand tree number density is 0.23 trees/m^2, and the tree trunk–main branch angle varies between 40° and 50°.

An observation point is placed at 0.5 m above the ground plane. For 200 Monte Carlo simulations of a sample forest stand consisting of 15 pine trees, which are randomly located around the observation point, the electric fields along the vertical and horizontal directions are computed. According to the experiment, an angle of incidence equal to 40° and illumination at 1.6 GHz is chosen. In this simulation, the reflected field from the ground has been excluded to be consistent with the measurement where the backscatter from a trihedral is used for the computation of two-way attenuation.

Fig. 1(a) and (b) compares the simulated and measured data where good agreement is shown. Here, L_h^2 and L_v^2 are the horizontal and vertical one-way foliage attenuation, respectively. The estimated mean values of the one-way attenuation factors reported in [27] are 9.31 dB for horizontal polarization and 9.16 dB for vertical polarization. These values computed by the simulation are about 9 dB for horizontal polarization and 9.4 dB for vertical polarization. The simulated values are within the precision of the measured data, i.e., ± 0.3 dB [27].

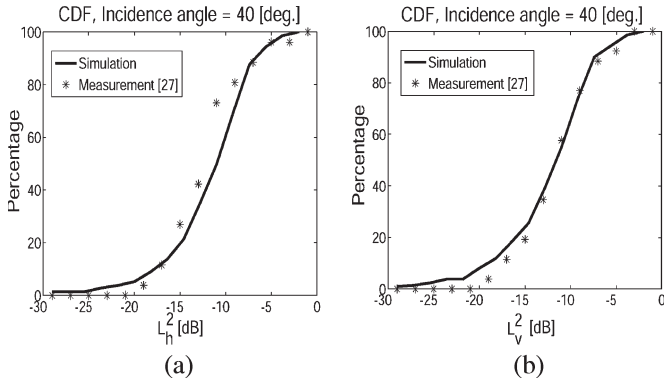

Fig. 1. Comparison between cdf of the simulated and measured one-way foliage attenuation for (a) horizontal and (b) vertical polarizations.

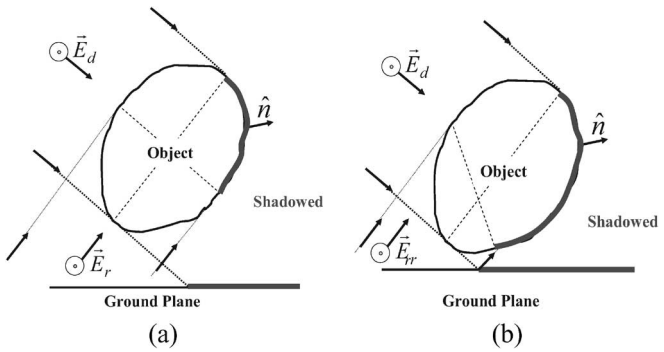

Fig. 2. Geometry of a smooth convex object and shadowed areas for direct and reflected waves for two different heights of the object above the ground plane.

III. Computation of Induced Surface Current

At very low frequencies, the scattering effect of the forest is rather small, and scattering behavior from the target is not much different from that of the target without the forest. As mentioned earlier, at high frequencies, the forest attenuates and distorts the incident wave phase front significantly. The computation of the scattered field from hard targets can be pursued in two different ways, namely: 1) exact numerical methods and 2) approximate analytic approaches [16]–[18]. Although exact numerical techniques can provide very accurate results, their utility is rather limited at high frequencies due to exorbitant computer memory and run times. This is especially true for the problem at hand where the number of sources illuminating the target can be as high as 10^5 or more.

Approximate analytic approaches, in turn, can be categorized into two methods, namely: 1) geometric theory of diffraction (GTD), which is based on ray tracing and computation of diffraction at discontinuities, and 2) PO, which is based on approximating the surface or volumetric currents on the scatterer. Noting that the number of scatterers around the target is very large, ray tracing and GTD are not computationally tractable. This difficulty is exasperated when the interaction of the scattered field from the hard target and nearby forest scatterers are needed as well. On the other hand, having tangential components of the incident fields over the target is sufficient to compute the PO currents. The PO approximation is known to produce valid scattered fields in directions near specular reflections off of scatterers, which tend to dominate other scattering mechanisms. For the problem at hand, we are dealing with a scattering scenario with multitudes of sources around the target. Therefore, for any scattering direction with a very high probability, there exists at least one specular reflection. This significantly improves the accuracy of the PO approximation.

A challenging step in establishing the PO currents on a hard target is the determination of the lit and shadowed points on complex target geometries. Again, ray tracing from each scatterer to the points on the target to determine whether they are lit or shadowed is a time-consuming task. To circumvent this difficulty, an iterative PO approach is considered, which can automatically account for shadowing effects. The iterative PO technique has been shown to be a very efficient high-frequency approach for capturing dominant near-field multiple-scattering effects (excluding edge effects) from electrically large targets [16]–[21].

To calculate the induced surface current on a metallic target embedded in a highly scattering environment, a hybrid method based on PO approximation is used. In this approach, first, the forest scattering model is used to find the electric and magnetic fields over the surface of the target. The magnetic field is then employed to calculate the induced surface current using Kirchhoff approximation. This approximation produces accurate results where the local radius of curvature at any point on the surface of the target is large compared to the wavelength. This approximation does not handle diffraction from the edges properly. Due to the existence of many scatterers around the target, the total scattered field from the target will be primarily dominated by the specular scattering contributions. Note that contributions from edge diffraction are significantly lower than scattering along specular directions.

To treat a complex object with PO approximation, the object is first decomposed into many small flat elementary patches, which have a simple geometry such as a rectangle or triangle. Then, using tangent plane approximation, the current on the lit region of the scatterer is approximated by [28]

$$\overline{J} \approx 2\hat{n} \times \overline{H} = \frac{-2i}{k_o Z_o} \hat{n} \times (\nabla \times \overline{E}) \tag{1}$$

where $\overline{E}$ and $\overline{H}$ are the incident electric and magnetic fields on the object, respectively, and $\hat{n}$ is the local normal unit vector as shown in Fig. 2. One difficulty encountered in determining the PO current of the target is identification of lit and shadowed facets. Another issue with the shadowing is the absence of the reflected rays from the ground because of the hard target itself. As shown in Fig. 2(a) and (b), the shadowed area on the target is a function of the target height above the ground. In what follows, procedures for dealing efficiently with the shadowing problem are introduced.

1) Simple Convex Object: Determination of lit and shadowed regions for convex objects is rather simple. Denoting the incidence direction from any scatterer in the forest to a point on the hard target or the direct incident wave by $\hat{k}_d$, the point is considered lit if $\hat{n} \cdot \hat{k}_d < 0$ and shadowed if $\hat{n} \cdot \hat{k}_d > 0$, as shown in Fig. 2. Here, $\hat{n}$ denotes the outward normal unit vector of the target surface. Due to the presence of the ground plane

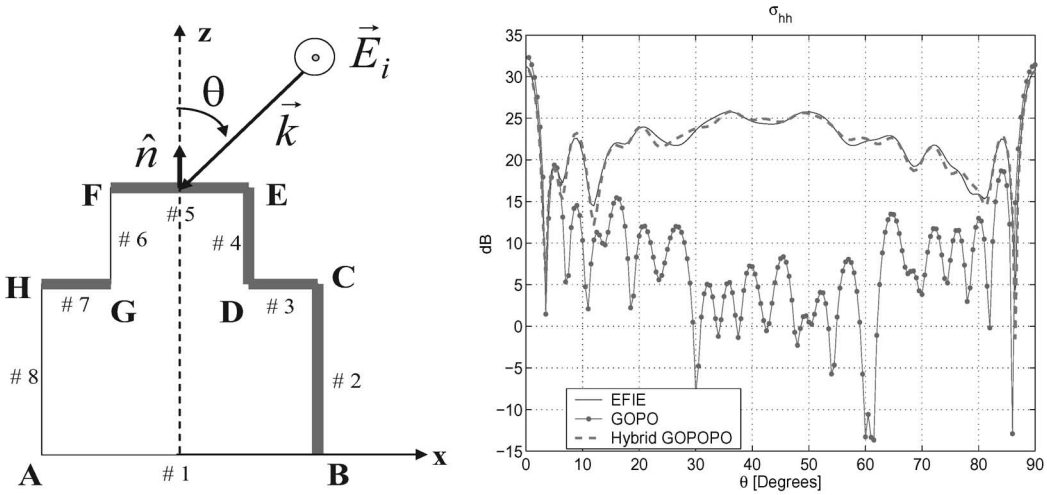

Fig. 3. (a) Geometry of a simple metallic target. (b) Comparison of backscattering RCS calculated by the exact EFIE method, the proposed hybrid GOPOPO method, and a first-order PO approximation (GOPO) for an H-polarized incident plane wave.

for every incident wave on the target, a reflected ray from the ground plane also exists. Denoting the direction of the reflected ray corresponding to $\hat{k}_d$, by $\hat{k}_r = \hat{k}_d - 2(\hat{z}\cdot\hat{k}_d)\hat{z}$, the lit and shadowed points can also be easily identified for the reflected rays. Generally, the blockage of the reflected rays by the target can be considered by ray tracing. To simplify this step, it is noted that for most practical problems, the target is sitting on the ground plane, and hence, the area directly underneath the target cannot produce reflected waves. This is important, since the total field on the target is composed of two mean fields (direct and reflected) plus four scattering terms from each scatterer. In situations where the ground reflection point happens to be just under the target, its contribution to the total field must be excluded. This is accomplished by placing a perfectly absorbing layer on the ground over the area where the target sits [29].

2) Complex Hard Target: As shown in the previous section, for simple convex objects, a GO approach can be used to find the lit and shadowed areas on the object, and PO can be used to find the surface electric current. This method henceforth will be referred to as the GOPO approach. However, this approach is not computationally efficient for targets with complex geometries, particularly when we consider the large number of illuminating sources around the target. For example, in a brute-force approach for a target with N_f discretized facets, the computation time for determining the lit or shadowed facets is proportional to N_f^2 for a single direction of incidence. Considering N_s scatterers around the target, the total computation time is proportional to $2N_sN_f^2$. The factor 2 here accounts for the fact that there exists an image for every scatterer in the ground plane. In addition, the GOPO accuracy for calculation of the radar cross section (RCS) may not be sufficient when near-field multiple bounces on the target itself are significant and/or typical dimensions of the scatterer become comparable with the wavelength [30]. For example, adjacent perpendicular facets on the target can form a dihedral, which can produce significant backscatter. Such contributions are not captured by a first-order PO approximation. A glance at the geometry of a typical target, as shown in Fig. 4(a), reveals the existence of such facets on the target.

To demonstrate this point, two simple objects such as two perfectly conducting boxes are considered (see Fig. 3). The induced surface current density on each point of the object can be calculated from the magnetic field integral equation (MFIE) [30] given by

$$\overline{J} = 2\hat{n}\times\overline{H}_i + 2\hat{n}\times L[\overline{J}] \tag{2}$$

where the operator $L[\cdot]$ is defined by

$$L[\overline{J}] = \int_{\text{surface}} (\overline{r}-\overline{r}')\times\overline{J}(r')\left(ik_0 - \frac{1}{|\overline{r}-\overline{r}'|}\right)\frac{e^{ik_0|\overline{r}-\overline{r}'|}}{4\pi|\overline{r}-\overline{r}'|^2}d\overline{r}'. \tag{3}$$

Near-field interaction of the surface currents on a target is responsible for certain scattering phenomena such as double-bounce scattering, in dihedral, or triple-bounce scattering, in corner reflector. In fact, a shadowing phenomenon can also be attributed to near-field interaction of surface currents. The current on the lit region produces a scattered field in the forward direction that is almost equal and out of phase with the incident wave. Hence, the sum of the scattered field and incident field over the shadowed region almost cancel each other, giving rise to a very small field there. The nonzero but small field in shadowed areas can be attributed to diffracted fields from the edges and shadow boundary [31]. This suggests that keeping track of multiple scattering can take care of shadowing problems automatically. In addition, effects of multiple scattering can be readily accounted for by an iterative PO approach.

Iterative PO has been used in the past to better estimate induced surface currents near shadow boundaries for convex objects [16], [17] or account for near-field multiple scattering for concave objects [18]–[20], [30]. Here, we use this approach to find shadow areas and capture higher order near-field scattering from complex targets embedded inside the foliage.

The starting point for the iterative PO solution is the MFIE given by (3). To the first-order approximation, we have $\overline{J}^{(1)} = 2\hat{n}\times\overline{H}_i$, which is the PO current. However, this approximation

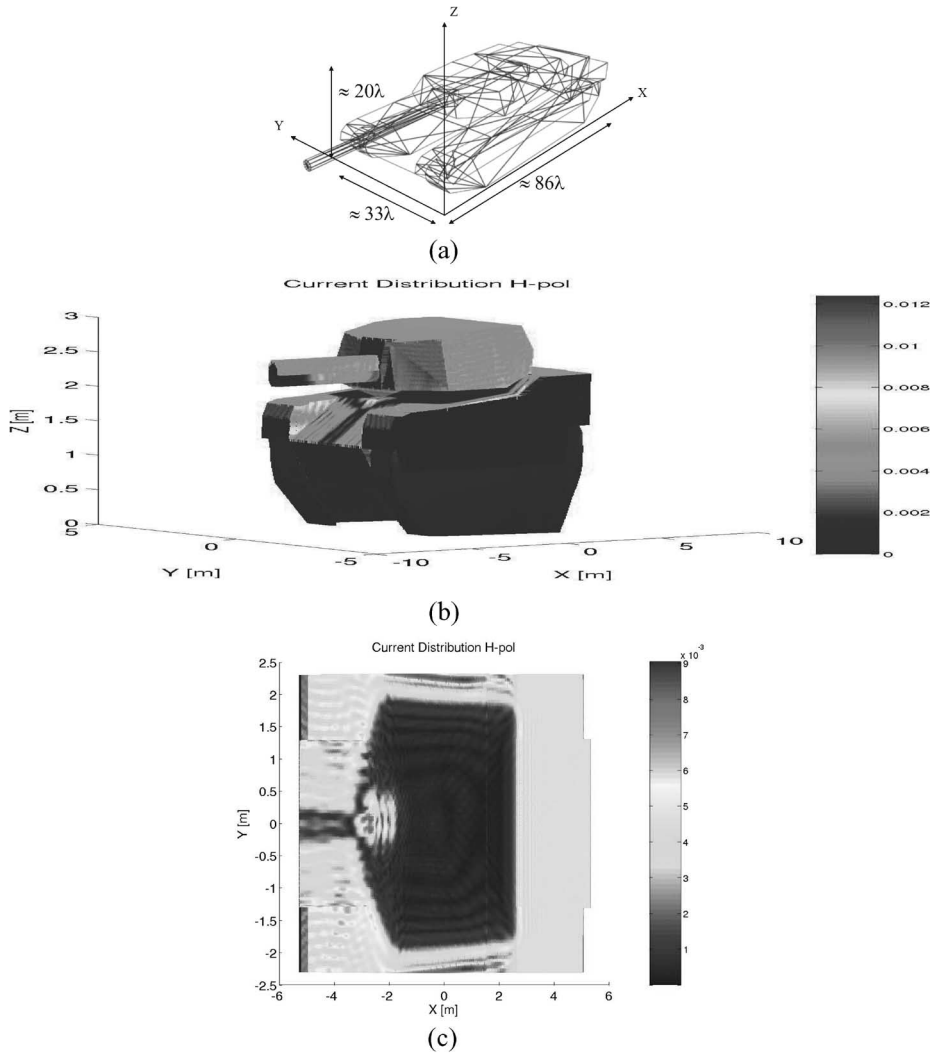

Fig. 4. (a) Structure and approximate dimensions of a simplified tank used for simulation at $f = 2$ GHz. (b) Electric current distribution over the hull of the tank with the turret removed. (c) Current distribution over the entire structure for an H-polarized incident wave in the direction of $\theta_i = 30^\circ$ and $\phi_i = 180^\circ$.

does not formally recognize the lit and shadowed areas. Instead of identifying the exact boundaries of the lit and shadowed areas over a complex target, a simple condition is used to find the primary shadowed areas first, and through a PO iteration, all shadowed areas are determined automatically. This procedure expedites the convergence of the iterative PO algorithm [20]. When calculating the field on the target for every source point, a primary shadowing condition given by $\hat{k} \cdot \hat{n} < 0$ is examined. Here, $\hat{k}$ is a unit vector from the source to the point on the surface. Of course, for complex objects, there are shadowed points (in concave regions) where $\hat{k} \cdot \hat{n} < 0$, but correct shadowing is achieved through iteration of the PO currents. Carrying on the iteration process, the same approach is taken for capturing the effect of higher order currents. That is, in computation of (3), only the contribution of the points where

$$(\overline{r} - \overline{r}') \cdot \hat{n} < 0 \tag{4}$$

is considered. In fact, (4), which is referred to as the shadowing rule, has been used in iterative PO approximations to find, for example, scattering from cavity structures [20]. Therefore, the second-order PO current given by

$$J^{(2)} = 2\hat{n} \times L\left[J^{(1)}\right] \tag{5}$$

will not only provide the double-bounce scattering over the lit region but also remove the first-order currents erroneously put over concave shadowed areas. Higher order currents can also be obtained in a similar manner, i.e., $J^{(m)} = 2\hat{n} \times L[J^{(m-1)}]$. For most practical applications, iteration up to the second order is sufficient. This second-order PO approach will be referred to as the hybrid GOPOPO method.

The iterative GOPOPO method in [30] proposes a ray-tracing approach (GO approximation) at its first step (first bounce) to determine the illuminated parts of each panel of a trihedral corner reflector. This is because the incident field is a plane wave (the target is in the far field of the source). This approach improves computation time as well as accuracy of the results, because it does not go through numerical computation of MFIE integral at the first step. However, as mentioned before, due to the large number of sources around the desired target,

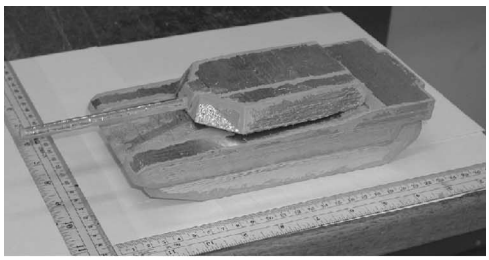

(a)

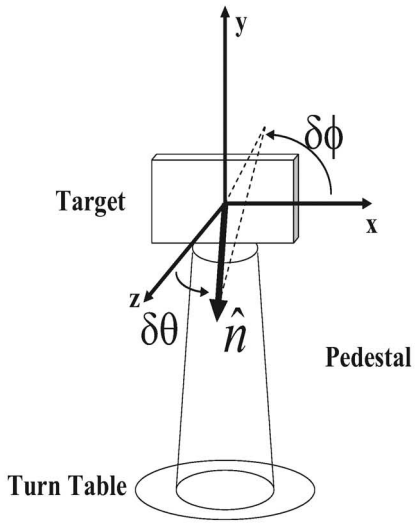

(b)

Fig. 5. (a) Scaled model for a surrogate tank used for backscatter measurements over the frequency range of 93–94 GHz. (b) Styrofoam target mount over a turntable for backscatter measurement. Here, $\hat{n}$ is the normal to the plate, and $\delta\theta$ and $\delta\phi$ denote target orientation errors.

determination of the illuminated areas for each source is not practically tractable.

To demonstrate this algorithm and its accuracy, let us consider the scatterer shown in Fig. 3(a). For a plane wave incidence, on facets # 2, # 3, # 4, # 5, and # 7 for which $\hat{n} \cdot \hat{k} < 0$, the first-order PO currents are placed initially. This is despite the fact that facet # 7 is partially or totally shadowed by facet # 5. The iterative PO should capture the double-bounce scattering mechanisms between facets # 4 and # 3, and correctly predict the shadowing of # 7 by facet # 5. To verify the proposed hybrid GOPOPO method, the backscatter of a PEC body shown in Fig. 3(a), with dimensions $AB = 8\lambda$, $BC = 4\lambda$, $CD = GH = 2.5\lambda$, and $DE = EF = 3\lambda$ and length of 10λ along the $\hat{y}$-direction at a frequency of 2 GHz, is compared with the backscatter RCS obtained from the method of moments (MoM) using an electric field integral equation (EFIE) formulation. The comparison is demonstrated in Fig. 3(b) for a transverse electric (TE) polarized wave, where very good agreement is shown. The discrepancies can be associated with the sharp edges of the object.

This method was also applied to a complex object such as a surrogate tank whose geometry is shown in Fig. 4(a). The target is first discretized into a triangular mesh whose sides are smaller than $\lambda/2$. For 2-GHz simulation, such a process renders 325 300 triangular facets on the target. The electric current distributions over the entire tank and over the hull are

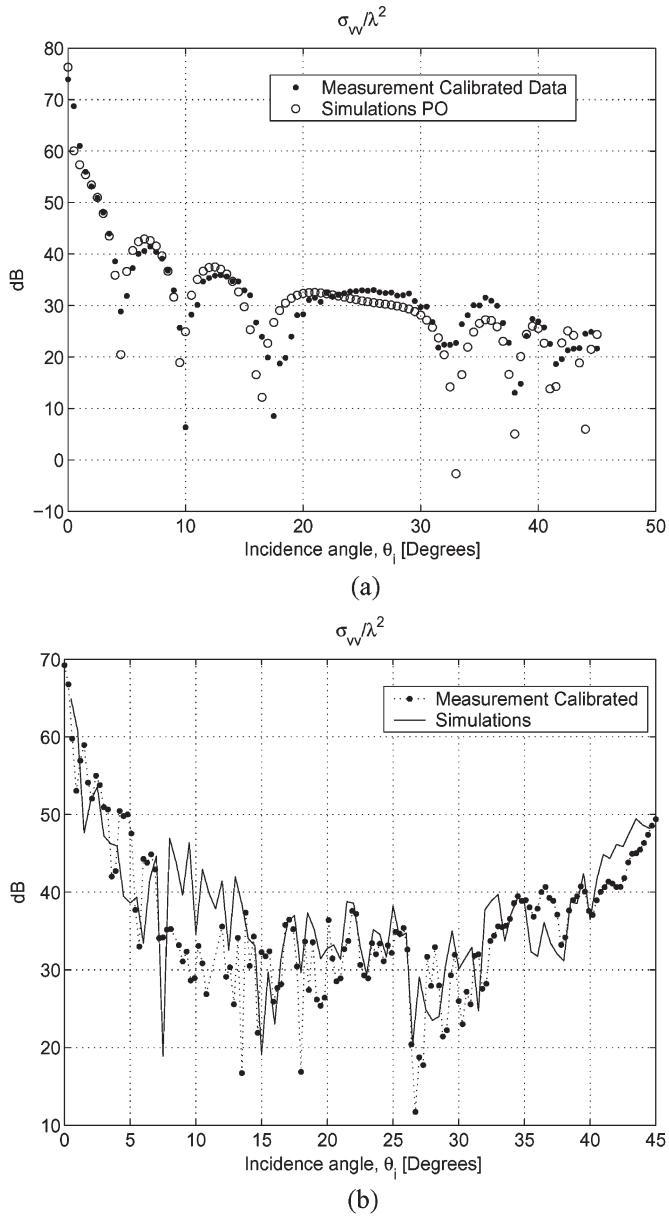

Fig. 6. Comparison of the backscattering RCS values between the measured and simulation results for (a) a rectangular PEC plate (20.3 × 9.5 cm) and (b) the scaled tank at $\phi_i = 180^\circ$ and different elevation incident angles of θ_i and for vertically polarized incident field.

shown in Fig. 4(b) and (c) for a horizontally polarized plane-wave illumination propagating along $\theta_i = 30^\circ$ and $\phi_i = 180^\circ$. The shadowed area on the top of the hull is generated by the turret roof and the gun, which is successfully predicted by the hybrid GOPOPO method.

It should be noted that there are advantages and disadvantages associated with the iterative PO approach. The advantages of the method are: 1) in comparison with full-wave analysis approaches such as MoM, there is no need to store or invert a very large matrix; 2) since it is based on high-frequency approximations much sparse discretization is needed [19]; and 3) depending on the structure of the target, the shadowing rule (4) can significantly reduce the number of required computations ($\propto N_f^2$). For example, for the structure shown in Fig. 3(a), where only the double-bounce scattering is dominant in the backscatter

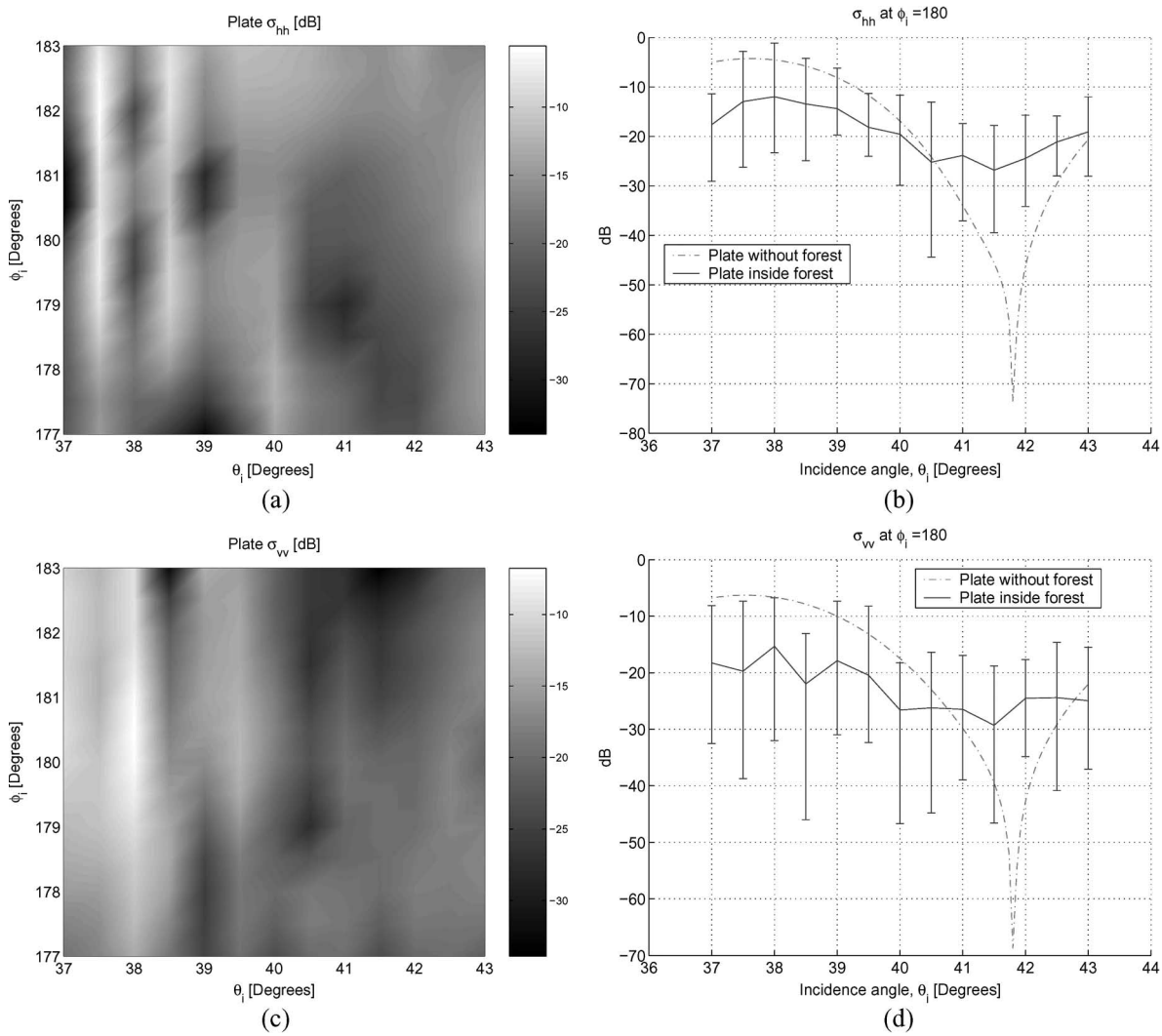

Fig. 7. Calculated RCS of a $3\lambda \times 3\lambda$ metallic plate over a lossy half-space embedded inside a pine forest canopy as a function of elevation and azimuth angles (a) $\sigma_{\rm hh}$ and (c) $\sigma_{\rm vv}$ at 2 GHz. Also shown is the backscatter from the plate with and without foliage at $\phi_i = 180^\circ$ and for different elevation angles. I-bar on the mean value shows the fluctuation range of the backscattering cross section for ten Monte Carlo simulations. (b) $\sigma_{\rm hh}$. (d) $\sigma_{\rm vv}$.

direction, the computation time is proportional to $0.11N_f^2$, where $N_f = 10\,182$. The main disadvantage of the iterative approach is that it may have a poor convergence, depending on the structure (the number of important reflections) and observation angles. Basically, for hard targets that have relatively deep concave parts such as cavity structures iterations may proceed to a large number, and for grazing angles to the aperture of the concave section, it may not even provide accurate results [19], [20]. However, for the type of structures at hand, noting that the target is being illuminated by myriads of nearby scatterers, it is expected that the iterative PO will provide satisfactory results.

A. Model Validation

To validate the simulated backscattering RCS of the tank, a scaled backscatter measurement at W-band frequencies is carried out. In this experiment, the University of Michigan's fully polarimetric W-band radar system, which operates over the frequency range of 93–94 GHz in a stepped-frequency mode, is used. A scaling factor of $s = 93.5/2 = 46.75$ is used to compare the measurements at 93.5 GHz with the simulation results at 2 GHz. A precise three-dimensional (3-D) printer is used to make the scaled tank model with an accuracy of a small fraction of a millimeter. The 3-D printer uses plaster as the building material; hence, metallic tapes are used to cover the structure. The fabricated prototype tank is shown in Fig. 5(a). The radar, which is used for measurement, is a coherent-on-receive system [32]. The receiver branch of the radar system has a dual-polarized antenna capable of measuring simultaneously the magnitudes and phases of both the vertical and horizontal polarizations of the scattered field. The transmitter is a single-port antenna that can transmit any arbitrary polarization. System distortion parameters can be measured using two calibration targets [32], namely a calibration sphere and any depolarizing target such as a 45° tilted cylinder. Knowing the distortion parameters, we can accurately measure the scattering matrix from any unknown target.

To verify the accuracy of the measurements, the RCS of a flat plate with a dimension of 20.3 × 9.5 cm is measured. In these measurements, an elaborate setup for target and radar alignment is needed. Basically, the RCSs of the targets that are composed of electrically large flat plates are very sensitive to the azimuth and elevation orientation angle errors [$\delta\theta$ and $\delta\phi$,

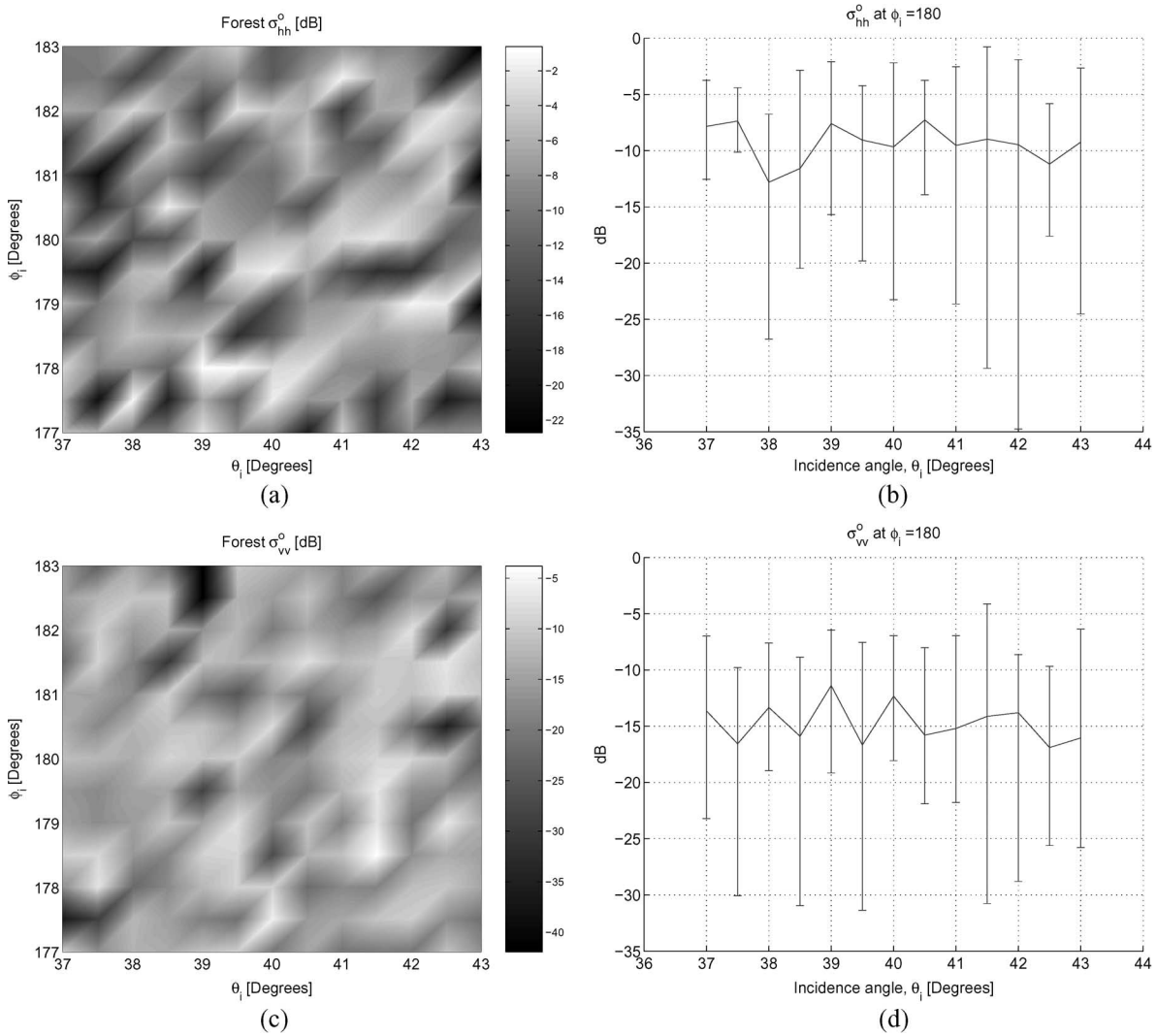

Fig. 8. Calculated backscattering coefficient of the pine stand as a function of elevation and azimuth angles of θ_i and ϕ_i. (a) $\sigma^o_{\rm hh}$. (c) $\sigma^o_{\rm vv}$. Also shown is the backscattering coefficient at $\phi_i = 180^\circ$ and for different elevation angles. I-bar on the mean value shows the fluctuation range of the backscattering coefficient for ten Monte Carlo simulations. (b) $\sigma^o_{\rm hh}$. (d) $\sigma^o_{\rm vv}$.

shown in Fig. 5(b)]. Fig. 6(a) presents the comparison between the measured and simulated backscatter from the flat plate where good agreement is shown. In addition, experiments have been repeated to ensure the repeatability of the measurements.

Fig. 6(b) shows a comparison between the measured and the simulated backscattered RCS of the tank using the proposed iterative PO approach for a vertical polarized incident wave at $\phi_i = 180^\circ$ and different values of θ_i. As shown, the iterative PO very closely follows the trend of the measured RCS. The discrepancies in the measured and simulated RCS values are typical of very large targets (in this case, $86\lambda \times 33\lambda \times 20\lambda$). Sources of the errors include the following: 1) target alignment with respect to the radar coordinate system (there are three degrees of freedom); 2) fabrication errors caused by shrinkage and warpage; and 3) errors caused by placement of metallic tapes and the seams. The effect of discretization is also examined by reducing the pixel area by a factor of 2.25, and no differences in the simulated results were noticed. The backscattered field from the tank target shown in Fig. 6(b) is provided for 90 elevation angles and three iterations per angle and computed using 16 AMD Athlon processors with a 2-GHz CPU and 1-GB RAM. The approximate time for each iteration is about 18 h.

IV. Computation of Hard Target–Foliage Interaction

The radar backscatter or bistatic scatter field may be decomposed into three basic components. One component of the scattered field emanates from the foliage directly. The second component can be viewed as the direct scattering from the target simply attenuated by the foliage above. This component retains the original signature of the target. Finally, the third component is composed of the scattered field interaction between the foliage and the target as well as the target and the foliage. In the previous section, the procedure for computation of surface currents on the hard target that includes the effect of scattering from nearby foliage was outlined. To compute the backscatter from the target directly, the dyadic Green's function in the presence of the trees is needed. Noting that the tree components are in the near-field region of the target, computation of the

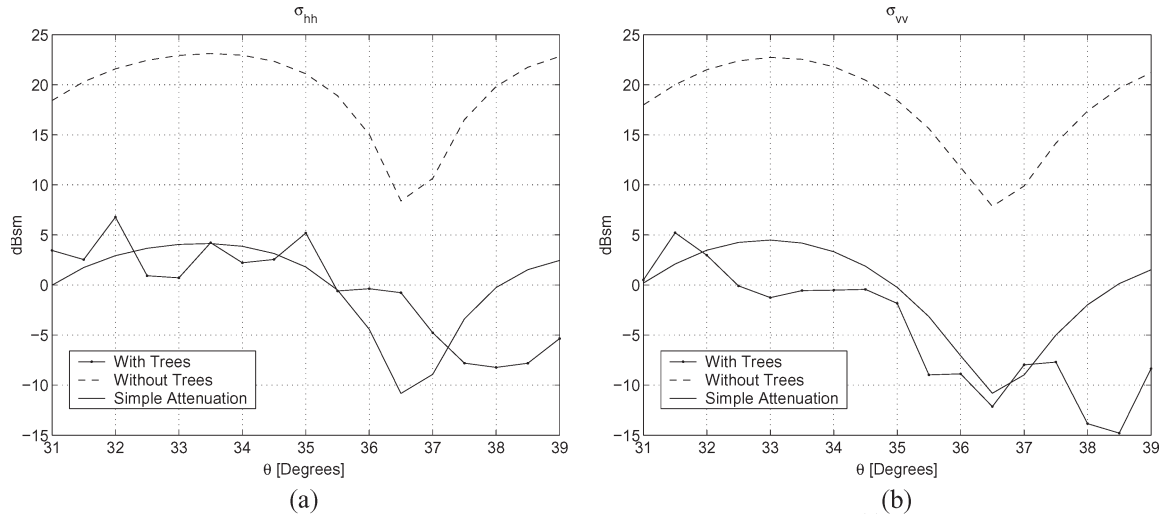

Fig. 9. Backscattered RCS of the metallic structure shown in Fig. 3, with dimensions of $AB = 8\lambda$, $BC = 4\lambda$, $CD = GH = 2.5\lambda$, and $DE = EF = 3\lambda$ and length of 5λ along the $\hat{y}$ direction, placed above a lossy dielectric ground at a frequency of 2 GHz, as a function of the incident angle θ_i for $\phi_i = 180^\circ$ inside and outside the forest. The density of pine trees is 0.05 trees/m^2. (a) $\sigma_{\rm hh}$. (b) $\sigma_{\rm vv}$. Direct backscatter from the forest is not shown in these figures.

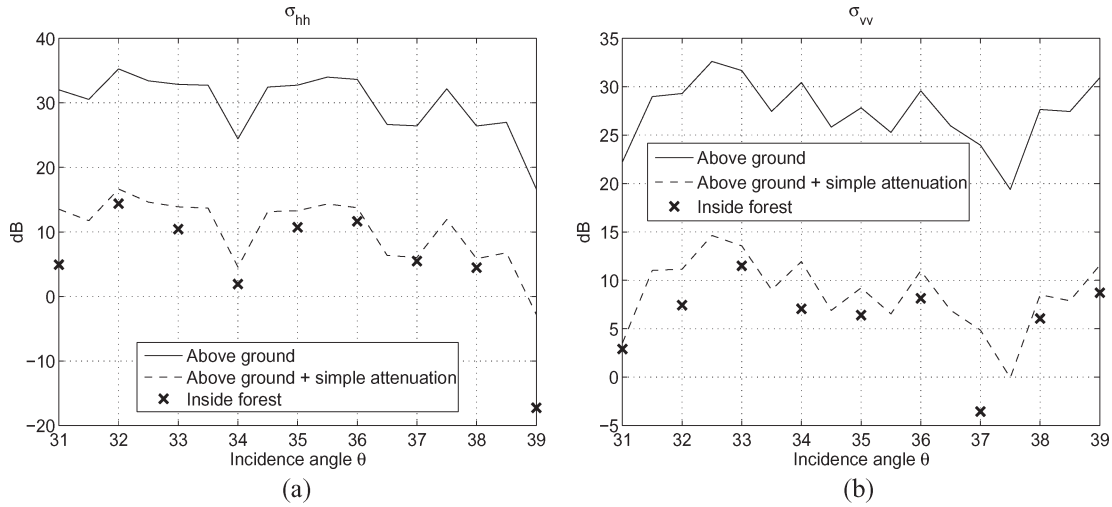

Fig. 10. Backscatter RCS of the metallic tank shown in Fig. 4(a) at a frequency of 2 GHz as a function of the incident angle θ_i for $\phi_i = 180^\circ$ with and without the effect of forest. (a) $\sigma_{\rm hh}$. (b) $\sigma_{\rm vv}$.

Green's function is very complex and time consuming. To simplify the calculation of the backscattered field from the target, inside the forest canopy, and account for the first-order target–foliage interaction, the reciprocity theorem is used.

The reciprocity theorem has been used in the past to account for first-order scattering interaction [14] and near-field to far-field transition [15]. In this approach, the induced currents and the total incident wave on the target, which are already computed, are needed to formulate the backscattered field. This way, foliage–target as well as target–foliage interactions can be accounted for simultaneously. According to the reaction theorem applied to a linear system composed of two sets of sources and fields, which are denoted by 1 and 2, we have [28]

$$\langle 1, 2\rangle = \langle 2, 1\rangle \tag{6}$$

where, for example, $\langle 2, 1\rangle$ denotes a surface or volume integral of the reaction of source 1, with the fields radiated from source 2 at the location of source 1.

For our problem, the incident field on the target is composed of the superposition of scattered fields from all tree constituents such as branches, trunks, and leaves and the direct field attenuated by the foliage (mean field). Each of these field components can be decomposed into a direct and a reflected field from the ground plane. Mathematically, this can be expressed as

$$\overline{E}_1 = (\overline{E}_d + \overline{E}_r)_{\rm mean} + \sum_{\rm Scatterers} (\overline{E}_d + \overline{E}_r) \tag{7}$$

where the subscripts d and r stand for the direct and reflected fields, respectively. Accordingly, the induced currents on the target, which are designated here as the second source, can be written as

$$\overline{J}_2 = (\overline{J}_d + \overline{J}_r)_{\rm mean} + \sum_{\rm Scatterers} (\overline{J}_d + \overline{J}_r). \tag{8}$$

TABLE I
RUN TIME REQUIRED FOR EACH REALIZATION OF THE FOREST AND EACH INCIDENCE ANGLE

	Num. of facets	Num. of scatterers	Processor [GHz]	RAM [GB]	Storage of currents	Run time
$Fig.7\ (b),(d)$	144	50000	2.0	0.5	Yes	1 $hour$
$Fig.9(a),(b)$	$7,534$	50000	2.0	1.0	No	1 day
$Fig.10(a),(b)$	$325,300$	10000	2.0	1.0	No	1 $week$

Considering an elementary electric current source, which is located at the point (radar position) $\overline{r}_R$, oriented along $-\hat{p}$, and having a magnitude given by

$$\overline{J}_1 = \frac{4\pi}{ik_oZ_o}\frac{r_R}{e^{ik_or_R}}\delta(\overline{r}-\overline{r}_R)(-\hat{p}) \tag{9}$$

the backscattered field $\overline{E}_2$ can be easily achieved [14]. Here, k_o and Z_o are the propagation constant and characteristic impedance of the free space, respectively. Since the target is assumed to be a perfect electric conductor (PEC), magnetic current is not considered. The unit vector $\hat{p}$ can be along $\hat{h}_i$ or $\hat{v}_i$, respectively, for horizontal or vertical polarization of the incident field, which is defined in a global coordinate system according to

$$\hat{h}_i = \frac{\hat{k}_i \times \hat{z}}{|\hat{k}_i \times \hat{z}|} \quad \hat{v}_i = \hat{h}_i \times \hat{k}_i \tag{10}$$

where $\hat{k}_i$ is the propagation unit vector of the incident field. With these assumptions, it can be shown that using (6), each component of the scattered field is expressed by

$$\mathbf{S}_{pq} = \pm\frac{ik_oZ_o}{4\pi}\int\limits_{\text{surface}} \overline{E}_{1p}\cdot\overline{J}_{2q}\,ds' \tag{11}$$

where the subscripts p and q can be h or v for horizontal and vertical polarizations. The first and second subscripts denote the receive and the transmit polarizations, respectively. Since for the backscattered field $\hat{k}_s = -\hat{k}_i$, we have $\hat{h}_s = -\hat{h}_i$ and $\hat{v}_s = \hat{v}_i$; therefore, the minus sign in (11) is chosen when p indicates vertical polarization.

Since both $\overline{E}_1$ and $\overline{J}_2$ are computed in the presence of the foliage around the target, the backscattered field computed from (11) also includes the interaction of target scattered fields with the foliage. It should be emphasized that the formulation given by (11) only accounts for the first-order scattering interaction between the hard target and foliage (and vice versa). Since in practice, there are sufficient separations between the hard target and foliage, first-order scattering captures most significant scattering interactions. This approach significantly simplifies backscatter field computation. Finally, the RCS of the target can be calculated from

$$\sigma^s_{pq} = 4\pi|\mathbf{S}_{pq}|^2. \tag{12}$$

V. SIMULATION OF HARD TARGETS EMBEDDED IN FOLIAGE

To examine the importance of foliage in modifying the RCS values and RCS signature of foliage-camouflaged targets, simulation of backscatter responses of simple targets in a pine forest is examined. First, we consider a $3\lambda \times 3\lambda$ horizontal metallic plate placed 1 m above a lossy ground plane. For this simulation, relative permittivity of the ground plane is set to $\epsilon_r = 5.6 + i0.8$, and the frequency of incident plane wave is chosen to be $f = 2$ GHz. For calculating the PO currents, the plate is meshed into 144 segments of $\lambda/4 \times \lambda/4$ square elementary patches over which the fields and the electric currents are considered constant. The backscatter RCS of the plate in the absence of forest using the reciprocity formula given by (11) is first compared with a closed-form PO expression [33]. In spite of small discrepancies, caused by discretization, excellent agreement is achieved for all incidence angles. Then, a complete simulation, including ten pine trees with a density of 0.05 trees/m^2 randomly located around the plate, is considered. Pine trees are generated by the statistical L-system having an average height of 15 m, a crown radius of 3 m, a crown height of 10 m, a trunk radius of 10 cm, and more than 5000 scatterers per tree.

Fig. 7(a) and (c) shows the plot of RCS of the plate alone inside the forest as a function of azimuth and elevation incident angles in steps of 0.5° for each angle. Strong fluctuation of RCS over a small angular range is indicative of significant foliage–target interaction. It is also interesting to observe that RCS variations along the elevation angle are more than those along the azimuth angle. To investigate the sensitivity of backscattered RCS from the plate to the tree arrangement, ten independent realizations of the pine forest are considered, and RCS values of the plate are computed. Fig. 7(b) and (d) shows the statistical behavior of the backscatter RCS from the plate alone at $\phi_i = 180°$ and for different elevation angles. The limits for the I-bars are the maximum and minimum RCS values observed in the realizations. As it appears, the attenuation and scattering from the forest particles reduce the average RCS and perturb the RCS pattern significantly. Constructive and destructive interferences result in substantial RCS fluctuations.

Similarly, Fig. 8(a) and (c) shows the RCS of the forest alone for different elevation and azimuth angles. It is observed that the average level of the backscattered signal from the forest as well as the fluctuation along the incident angles is higher than that of the plate. As shown in Fig. 8(b) and (d), the backscattering coefficient of the forest is almost constant over the angular range of incidence angle. The backscattering coefficient for vertical polarization (σ^o_{vv}) is about 5 dB less than that for horizontal polarization (σ^o_{hh}). This is caused by the reduction in the RCS of the ground–trunk component for vertical polarization due to the Brewster angle effect on tree trunks. In conclusion, changing the elevation or azimuthal incident angles or realization of the trees around the target has similar effects with changing the RCS of the plate. These

simulations clearly indicate that simply modeling a forest by an attenuation layer fails to predict such strong RCS fluctuations, which are caused by the interaction of foliage with the target and vice versa.

Fig. 9(a) and (b) compares the backscatter from a metallic structure, as shown in Fig. 3(a), having dimensions of $AB = 8\lambda$, $BC = 4\lambda$, $CD = GH = 2.5\lambda$, and $DE = EF = 3\lambda$ and length of 5λ along the $\hat{y}$ direction, placed above a lossy dielectric ground plane, as a function of the incident angle θ_i at $\phi_i = 180^\circ$ for one realization of the pine forest. Frequency of operation is set to 2 GHz. Due to the presence of tree trunks, in forward scattering, a horizontally polarized wave has more penetration through the foliage than the vertically polarized wave. Therefore, as shown in Fig. 9, it is observed that the average target RCS at horizontal polarization is higher than that at vertical polarization. Fig. 10(a) and (b) compares the backscatter from the metallic tank, as shown in Fig. 4(a). In this simulation, the scattering effect of two adjacent trees, which are located at (7,0) and $(-7,3)$, are taken into account.

It is observed that this hybrid target–foliage model is capable of simulating a large domain of computations. The run time is basically determined by the number of discretized facets, the structure of the target, the number of included trees (scatterers) around the target, the frequency of operation, and the processors' features. In addition, the run time would increase if the fields or currents on the target are intended for storage. In fact, simulations provided in this paper are run by a personal computer, and more complicated and larger targets can be simulated using parallel computers. Table I shows the estimated run time of simulations provided in this paper for each realization of forest and each incidence angle. It should be noted that for simulation of the plate, as shown in Fig. 7, 169 different angles, and for each angle, ten different realizations of the forest have been considered.

Comparing the forest backscatter obtained from σ^o, as shown in Fig. 8 multiplied by the radar footprint or pixel area, with that of the target shown in Fig. 9, the signal-to-clutter ratio may be a small quantity, depending upon the pixel area. To enhance the signal-to-clutter ratio, the polarization signature of the target and the clutter can be studied to discriminate the target backscatter response from that of the clutter.

VI. Conclusion

A novel computationally efficient hybrid target–foliage model is developed for investigating methods for detecting foliage-camouflaged targets. The model is based on the reciprocity theorem for calculation of backscattering and a hybrid GOPOPO method for efficient calculation of induced currents on hard targets embedded in the foliage. The proposed method for calculation of RCS is verified using the MoM and RCS measurement of a scaled model at millimeter-wave frequencies. In addition, a sensitivity study has been carried out to demonstrate the sensitivity of the backscatter from metallic targets under forest canopies to the polarization, incidence angle, and forest realizations. The results clearly indicate the significance of the scattering from tree components on the target response at the microwave frequencies as low as 2 GHz.

References

[1] D. J. Blejer, S. M. Scarborough, C. E. Frost, H. R. Catalan, K. H. McCoin, J. Roman, and D. M. Mukai, "Ultra-wideband polarimetric imaging of corner reflectors in foliage," in *Proc. IEEE Antennas and Propag.*, Jul. 1992, pp. 587–590.

[2] F. T. Ulaby and C. Elachi, *Radar Polarimetry for Geoscience Applications*. Norwood, MA: Artech House, 1990.

[3] G. A. Ioannidis and D. E. Hammers, "Optimum antenna polarizations for target discrimination in clutter," *IEEE Trans. Antennas Propag.*, vol. AP-27, no. 3, pp. 357–363, May. 1979.

[4] G. Zhang and L. Tsang, "Application of angular correlation function of clutter scattering and correlation imaging in target detection," *IEEE Trans. Geosci. Remote Sens.*, vol. 36, no. 5, pp. 1485–1493, Sep. 1998.

[5] T.-K. Chan, Y. Kuga, and A. Ishimaru, "Experimental studies on circular SAR imaging in clutter using angular correlation function technique," *IEEE Trans. Geosci. Remote Sens.*, vol. 37, no. 5, pp. 2192–2197, Sep. 1999.

[6] M. L. Imhoff, "A theoretical analysis of the effect of forest structure on SAR backscatter and the remote sensing of biomass," *IEEE Trans. Geosci. Remote Sens.*, vol. 33, no. 2, pp. 341–352, Mar. 1995.

[7] Y.-C. Lin and K. Sarabandi, "A Monte Carlo coherent scattering model for forest canopies using fractal-generated trees," *IEEE Trans. Geosci. Remote Sens.*, vol. 37, no. 1, pp. 440–451, Jan. 1999.

[8] C. D. Moss, F. L. Teixeira, Y. Eric Yang, and J. A. Kong, "Finite-difference time-domain simulation of scattering from objects in continuous random media," *IEEE Trans. Geosci. Remote Sens.*, vol. 40, no. 1, pp. 178–186, Jan. 2002.

[9] H. Israelsson, L. M. H. Ulander, T. Martin, and J. I. H. Askne, "A coherent scattering model to determine forest backscattering in VHF-band," *IEEE Trans. Geosci. Remote Sens.*, vol. 38, no. 1, pp. 238–248, Jan. 2000.

[10] A. Y. Nashashibi and F. T. Ulaby, "Detection of stationary foliage-obscured targets by polarimetric millimeter-wave radar," *IEEE Trans. Geosci. Remote Sens.*, vol. 43, no. 1, pp. 13–23, Jan. 2005.

[11] A. Y. Nashashibi, K. Sarabandi, S. Oveisgharan, M. C. Dobson, W. S. Walker, and E. Burke, "Millimeter-wave measurements of foliage attenuation and ground reflectivity of tree stands at nadir incidence," *IEEE Trans. Antennas Propag.*, vol. 52, no. 5, pp. 1211–1222, May 2004.

[12] J. G. Fleischman, S. Ayasli, E. M. Adams, and D. R. Gosselin, "Foliage attenuation and backscatter analysis of SAR imagery," *IEEE Trans. Aerosp. Electron. Syst.*, vol. 32, no. 1, pp. 135–144, Jan. 1996.

[13] I.-S. Koh and K. Sarabandi, "Polarimetric channel characterization of foliage for performance assessment of GPS receivers under tree canopies," *IEEE Trans. Antennas Propag.*, vol. 50, no. 5, pp. 713–726, May 2002.

[14] K. Sarabandi and P. F. Polatin, "Electromagnetic scattering from two adjacent objects," in *Proc. PIERS*, Pasadena, CA, Jul. 1993, p. 606.

[15] K. Demarest, Z. Huang, and R. Plumb, "An FDTD near- to far-zone transformation for scatterers buried in stratified ground," *IEEE Trans. Antennas Propag.*, vol. 44, no. 8, pp. 1150–1157, Aug. 1996.

[16] M. Kaye, P. K. Murthy, and G. A. Thiele, "An iterative method for solving scattering problems," *IEEE Trans. Antennas Propag.*, vol. AP-33, no. 11, pp. 1272–1279, Nov. 1985.

[17] P. K. Murthy, K. C. Hill, and G. A. Thiele, "A hybrid-iterative method for scattering problems," *IEEE Trans. Antennas Propag.*, vol. AP-34, no. 10, pp. 1173–1180, Oct. 1986.

[18] T. Griesser and C. A. Balanis, "Backscatter analysis of dihedral corner reflectors using physical optics and physical theory of diffraction," *IEEE Trans. Antennas Propag.*, vol. AP-35, no. 10, pp. 1137–1147, Oct. 1987.

[19] F. Obelleiro, J. L. Rodriguez, and R. J. Burkholder, "An iterative physical optics approach for analyzing the electromagnetic scattering by large open-ended cavities," *IEEE Trans. Antennas Propag.*, vol. 43, no. 4, pp. 356–361, Apr. 1995.

[20] R. J. Burkholder, "A fast and rapidly convergent iterative physical optics algorithm for computing the RCS of open-ended cavities," *Appl. Comput. Electromagn. Soc. J.*, vol. 16, no. 1, pp. 53–60, Mar. 2001.

[21] K. Sarabandi and M. Park, "A radar cross-section model for power lines at millimeter-wave frequencies," *IEEE Trans. Antennas Propag.*, vol. 51, no. 9, pp. 2353–2360, Sep. 2003.

[22] L. Tsang, J. A. Kong, and R. T. Shin, *Theory of Microwave Remote Sensing*, ser. Wiley Series in Remote Sensing. New York: Wiley, 1985.

[23] M. A. Karam, A. K. Fung, R. H. Lang, and N. S. Chauhan, "A microwave scattering model for layered vegetation," *IEEE Trans. Geosci. Remote Sens.*, vol. 30, no. 4, pp. 767–784, Jul. 1992.

[24] F. T. Ulaby, K. Sarabandi, K. McDonald, M. Whitt, and M. C. Dobson, "Michigan Microwave Canopy Scattering Model (MIMICS)," Univ. Michigan, Ann Arbor, Tech. Rep. 022486-T-1, Jul. 1988.

[25] K. Sarabandi, "Electromagnetic scattering from vegetation canopies," Ph.D. dissertation, Dept. Elect. Eng. Comput. Sci., Univ. Michigan, Ann Arbor, 1989.
[26] L. Tsang, J. A. Kong, and K.-H. Ding, *Scattering of Electromagnetic Waves: Theories and Applications*, ser. Wiley Series in Remote Sensing. Hoboken, NJ: Wiley, 2000.
[27] F. T. Ulaby, M. W. Whitt, and M. C. Dobson, "Measuring the propagation properties of a forest canopy using a polarimetric scatterometer," *IEEE Trans. Antennas Propag.*, vol. 38, no. 2, pp. 251–258, Feb. 1990.
[28] R. F. Harington, *Time-Harmonic Electromagnetic Fields*. New York: Wiley, 2001.
[29] M. Dehmollaian and K. Sarabandi, "A forward scattering model for foliage camouflaged complex targets," in *Proc. IGARSS*, Sep. 20–24, 2004, vol. 1.
[30] K. Sarabandi and T.-C. Chiu, "Optimum corner reflectors for calibration of imaging radars," *IEEE Trans. Antennas Propag.*, vol. 44, no. 10, pp. 1348–1361, Oct. 1996.
[31] M. D. Casciato and K. Sarabandi, "High frequency radio wave diffraction from singly curved surfaces: A heuristic approach," *Proc. Inst. Elect. Eng.—Microw. Antennas Propag.*, vol. 151, no. 1, pp. 43–53, Feb. 2004.
[32] A. Nashashibi, K. Sarabandi, and F. T. Ulaby, "A calibration technique for polarimetric coherent-on-receive radar system," *IEEE Trans. Antennas Propag.*, vol. 43, no. 4, pp. 396–404, Apr. 1995.
[33] H. T. Anastassiu, "Radar cross section of a perfectly conducting, flat, polygonal plate over a dielectric, lossy half-space: A closed form, physical optics expression," in *Proc. Int. Conf. Math. Methods Electromagn. Theory*, Sep. 2002, vol. 2, pp. 505–507.

Mojtaba Dehmollaian (S'04) was born in Iran, in 1978. He received the B.S. and M.S. degrees in electrical engineering from the University of Tehran, Tehran, Iran, in 2000 and 2002, respectively. He is currently working toward the Ph.D. degree as a Research Assistant graduate student at the Radiation Laboratory, University of Michigan, Ann Arbor.

His research interests are in the area of applied computational electromagnetics with particular interest in remote sensing.

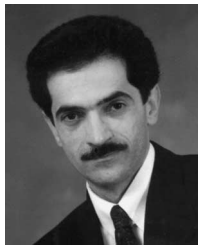

Kamal Sarabandi (S'87–M'90–SM'92–F'00) received the B.S. degree in electrical engineering from Sharif University of Technology, Tehran, Iran, in 1980, the M.S. degree in electrical engineering, in 1986, the M.S. degree in mathematics, and the Ph.D. degree in electrical engineering from The University of Michigan, Ann Arbor, in 1989.

He is currently the Director of the Radiation Laboratory and a Professor at the Department of Electrical Engineering and Computer Science, University of Michigan. His research areas of interest include microwave and millimeter-wave radar remote sensing, metamaterials, electromagnetic wave propagation, and antenna miniaturization. He has 20 years of experience with wave propagation in random media, communication channel modeling, microwave sensors, and radar systems and is leading a large research group including two research scientists, 12 Ph.D., and two M.S. students. He has graduated 23 Ph.D. and supervised numerous postdoctoral students. He has served as the Principal Investigator on many projects sponsored by the National Aeronautics and Space Administration, Jet Propulsion Laboratories, Army Research Office, Office of Naval Research, Applied Research Laboratory, National Science Foundation, Defense Advanced Research Projects Agency, and a larger number of industries. He has published many book chapters and more than 135 papers in refereed journals on EM-scattering, random media modeling, wave propagation, antennas, metamaterials, microwave measurement techniques, radar calibration, inverse scattering problems, and microwave sensors. He has also had more than 330 papers and invited presentations in many national and international conferences and symposia on similar subjects.

Dr. Sarabandi is a Vice President of the IEEE Geoscience and Remote Sensing Society (GRSS), and a member of IEEE Technical Activities Board Awards Committee. He served as the Associate Editor of the IEEE TRANSACTIONS ON ANTENNAS AND PROPAGATION (AP) and the IEEE SENSORS JOURNAL. He is also a member of Commissions F and D of the Union Radio Scientific International (URSI) and of The Electromagnetic Academy. He is listed in American Men and Women of Science Who's Who in America and Who's Who in Science and Engineering and was the recipient of the Henry Russel Award from the Regent of The University of Michigan (the highest honor The University of Michigan bestows on a faculty member at the assistant or associate level). In 1999, he received a German American Academic Council Distinguished Lecturer Award from the German Federal Ministry for Education, Science, and Technology given to about ten individuals worldwide in all areas of engineering, science, medicine, and law. He was also a recipient of a 1996 Electrical Engineering and Computer Science Department Teaching Excellence Award and a 2004 College of Engineering Research Excellence Award. In 2005, he received two prestigious awards, namely, the IEEE Geoscience and Remote Sensing Distinguished Achievement Award and The University of Michigan Faculty Recognition Award. In the past several years, joint papers presented by his students at a number of international symposia (IEEE Antennas and Propagation Society (APS)'95, '97, '00, '01, '03, '05; IEEE International Geoscience and Remote Sensing Symposium (IGARSS)'99, '02, IEEE International Microwave Symposium (IMS)'01, United States National Committee (USNC) International Union for Radio Science (URSI)'04, '05, '06) have received Best Student Prize Paper Awards.